Influence of Polymer End Groups on Crystallization and Morphology of Poly(vinylidene fluoride) Synthesized in Homogeneous Phase with Supercritical Carbon Dioxide

Muhammad Imran-ul-haq, Brigitte Tiersch, and Sabine Beuermann*

Institute of Chemistry, University of Potsdam, Karl-Liebknecht Strasse 24-25, 14476 Golm/Potsdam, Germany

Received December 7, 2007; Revised Manuscript Received August 12, 2008

ABSTRACT: Poly(vinylidene fluoride) (PVDF) samples from homogeneous phase polymerizations in supercritical CO_2 and subsequent expansion to ambient conditions were analyzed with respect to polymer end groups, crystallinity, type of polymorphs, and morphology. Upon expansion the polymer was obtained as white particles. Scanning electron microscopy showed that DTBP (di-*tert*-butyl peroxide) derived polymer end groups lead to stack-type particles whereas sponge- or rose-type particles were obtained in case of chain transfer agent fragments as end groups. FTIR (Fourier-transform infrared spectroscopy) and WAXD (wide-angle X-ray diffraction) indicated that the type of polymorph, α or β crystal phase, is significantly affected by the type of end group. In addition, the crystallinity of the material, as determined via differential scanning calorimetry, is affected by the end groups and polymer molecular weights. For example, with M_n around 6700 g·mol^{-1} crystallinity ranges from 29% for DTBP-derived endgroups to a maximum of 64% for end groups originating from perfluorinated hexyl iodide used as chain transfer agent during polymerization.

Introduction

PVDF is known to be a semicrystalline polymer with five different polymorphs, the so-called α, β, γ, δ, and ϵ forms.[1] The occurrence of these PVDF polymorphs strongly depends on polymerization conditions and processing of the polymer, e.g., thermal treatment or application of an electrical field. Further, it was shown that polymer morphology may be affected by the use of supercritical carbon dioxide ($scCO_2$).[2] The different crystal phases are associated with widely varying polymer properties, e.g. the β phase has piezo- and pyroelectric properties.[3] The correlation of crystalline structure and resultant electrical properties has led to several studies in which it was attempted to prepare different phases by altering thermal history,[4] mechanical deformation,[5] γ irradiation,[6] or pressure.[7] In addition, PVDF shows low acoustic impedance.[8] Polymeric piezoelectrics were used, e.g. as energy converters and different types of sensors in medicine. While pure PVDF has a modest dielectric permittivity, recently it was shown that hybrid materials consisting of PVDF and carbon nanotubes show very high permittivities that may find potential applications as actuators for artificial muscles.[9] Further attractive applications of VDF homo- and copolymers and are seen as membranes[10−12] for filtration or for fuel cells.

To date homo- and copolymers of vinylidene fluoride (VDF) are mostly obtained from reactions in heterogeneous aqueous phase employing fluorinated surfactants, which allow for excellent stabilization. However, stabilizers like, e.g., ammonium perfluorooctanoate are persistent and were reported to accumulate in nature.[13] Thus, there is a strong need for new processes that do not employ fluorinated surfactants. Liquid and supercritical CO_2 are regarded as promising alternate reaction media for innovative syntheses of fluoropolymers.[14−27] Particularly interesting are processes that do not employ stabilizers, such as precipitation or solution polymerizations in $scCO_2$.

Although polymer solubility is generally rather low in $scCO_2$,[28] some polymers with carbonyl groups,[29,30] ether moieties,[31,32] or CF bonds[33−35] undergo specific interactions with CO_2 that give rise to CO_2 dissolution in the polymers, to plasticization of the amorphous phase, or to depression of the melting temperature of the crystalline phase. Recently, we showed that VDF may be polymerized in $scCO_2$ in homogeneous phase using di-*tert*-butyl peroxide (DTBP) as initiator.[26] After complete monomer conversion was reached expansion of the reaction mixture to ambient pressure conditions resulted in dry polymer material consisting of stack-like particles. Additional VDF polymerizations were carried out in the presence of perfluorohexyl iodide serving as a degenerative chain-transfer agent.[27] Again, expansion of the reaction mixtures after polymerization up to complete monomer conversion was finalized resulted in particulate material. However, the visual appearance of these particles was different from the particles with DTBP-derived end groups. While it is well-known that thermal stability or fire resistance of polymers are dependent on end groups, a significant influence of polymer end groups on polymer bulk properties is rather surprising. It was reported that fluidity and electrical conductivity of PVDF as well as crystallization kinetics from the melt associated with processing and end-use properties of thermoplastic fluoropolymers may be influenced by the polymer end groups.[36] Herman et al. reported that PVDF with CCl_4-derived end groups does not only show a higher melting temperature than PVDF of the same chain length but with initiator-derived end groups, further the dominating crystal phase was affected by the type of end group.[37] However, the crystal phase assignment was based on IR spectra and X-ray diffraction measurements of polymers casted from acetone solution onto silicon wafers. While some differences between the samples were visible, it is not possible to draw conclusions for the bulk material.

Thus, we were interested in studying how polymer end groups of PVDF affect the bulk and surface morphology as well as the melting and crystallization behavior of the polymer. Polymers under investigation were obtained from homogeneous phase reactions in $scCO_2$ with molecular weight control via initiation using DTBP or via chain transfer employing either perfluorinated hexyl iodide or bromotrichloromethane. The polymers were analyzed by means of scanning electron microscopy (SEM),

* To whom correspondence should be addressed: E-mail: sabine.beuermann@uni-potsdam.de. Telephone: +49-331-977-5228. Fax: +49-331-977-5059.

10.1021/ma801325p CCC: $40.75
Published on Web 10/04/2008

Table 1. Poly(vinylidene fluoride) Samples Employed[a]

sample	appearance	MW control	end groups	M_n (g·mol^{-1})	M_w/M_n
DTBP-1[b]	fine powder	$c_{DTBP} = 0.307$ mol·L^{-1}	CH_3	2200	4.5
DTBP-2[b]	fine powder	$c_{DTBP} = 0.077$ mol·L^{-1}	CH_3	6800	3.1
PFHI-1[c]	fine powder	$c_{PFHI} = 0.150$ mol·L^{-1} [d]	I, $CF_3(CF_2)_5$	2400	1.4
PFHI-2[c]	fine powder	$c_{PFHI} = 0.050$ mol·L^{-1} [d]	I, $CF_3(CF_2)_5$	6700	1.5
BTCM-1[c]	coagulated polymer	$c_{BTCM} = 0.921$ mol·L^{-1} [d]	Br, CCl_3	2100	1.6
BTCM-2[c]	fine powder	$c_{BTCM} = 0.230$ mol·L^{-1} [d]	Br, CCl_3	6000	1.6

[a] Number average molecular weights, M_n, and weight average molecular weights, M_w, were obtained from size exclusion chromatography with polystyrene calibration. [b] Polymerization at 140 °C, 1500 bar [c] Polymerization at 120 °C, 1500 bar. [d] Concentration of di-*tert*-butyl peroxide (c_{DTBP}) $c_{DTBP} = 0.061$ mol·L^{-1}. c_{PFHI} and c_{BTCM}: concentrations of $C_6F_{13}I$ and CCl_3Br, respectively. The monomer concentration was always 3.6 mol·L^{-1}.

atomic force microscopy (AFM), Fourier transform infrared spectroscopy (FTIR), wide-angle X-ray diffraction (WAXD) and differential scanning calorimetry (DSC).

Experimental Section

Chemicals. All reactions were carried out with the monomer vinylidene fluoride (VDF, Solvay Solexis), carbon dioxide (CO_2, grade 4.5, Messer Griesheim), and di-*tert*-butyl peroxide (DTBP, Akzo Nobel) as initiator. Polymer molecular weights were controlled by the chain-transfer agents perfluorinated hexyl iodide ($C_6F_{13}I$, Dyneon), perfluorinated octyl iodide ($C_8F_{17}I$, Dyneon) and bromotrichloromethane (CCl_3Br, Acros, 99%). All chemicals were used as received.

Polymerizations. VDF polymerizations in solution with around 73 wt.% CO_2 were carried out at 120 °C and 1500 bar with 0.061 mol·L^{-1} DTBP in the presence of either CCl_3Br or $C_6F_{13}I$. Chain-transfer agent concentrations were chosen to yield polymer samples with M_n around 2200 g·mol^{-1} and 6000 g·mol^{-1} (see Table 1). PVDF samples with DTBP-derived end groups were obtained from reactions at 140 °C and 1500 bar in 73 wt.% CO_2 in the absence of any chain transfer agents. PVDF with $M_n = 2200$ g·mol^{-1} and $M_n = 6800$ g·mol^{-1} were synthesized with DTBP concentrations of 0.307 and 0.077 mol·L^{-1}, respectively. All polymerizations were carried out with a monomer concentration of around 3.6 mol·L^{-1} according to the detailed descriptions in our previous publications.[26,27] The polymers were characterized according to the following procedures.

Molecular Weight Distributions. Size-exclusion chromatography (SEC) of the polymers was carried out with *N*,*N*-dimethyl acetamide (DMAc) containing 0.1% LiBr as eluent and a column temperature of 45 °C. The samples were analyzed on a SEC setup consisting of an Agilent 1200 isocratic pump, an Agilent 1200 refractive index detector, and two GRAM columns (10 μm, 8 × 300 mm, pore sizes 100 and 1000) from Polymer Standards Services. The SEC setup was calibrated using low polydispersity polystyrene standards (PSS), since PVDF standards were not available.

End Group Analyses. ^{1}H NMR spectra of PVDF dissolved in acetone-d_6 were recorded on a Bruker 300 MHz spectrometer to determine the polymer end groups. In addition, ESI−MS (electrospray ionization mass spectrometry) was performed. The ESI spectra were recorded using a Q-TOF micro mass spectrometer (Micromass Manchester, UK) in positive ion mode. The samples were injected (20 mL·min^{-1}) using a Harvard syringe pump. The capillary voltage was set to 2.7 kV and the cone voltage within the range of 25 V. The source temperature was 80 °C and the desolation temperature 150 °C. The ESI mass spectra (positive ion mode) were measured for PVDF in $CHCl_3$ with CH_3OH.

Thermal Analyses. Differential scanning calorimetry (DSC 2010, TA Instruments) was used to measure melting temperatures and melting enthalpies of the PVDF samples. For each sample, three heating−cooling cycles were measured. For the determination of the degree of crystallinity the DSC data recorded during the second cycle were analyzed. The temperature was varied from 0 to 200 °C with a heating rate of 10 °C per minute. PVDF crystallinity, *X*, was calculated according to eq 1

$$X = \Delta H/\Delta H_c \times 100\ (\%) \quad (1)$$

where $\Delta H_c = 104.5$ J·g^{-1} is the melting enthalpy for a 100% crystalline sample of PVDF.[38]

Determination of PVDF Polymorphs. To determine the crystalline phases of the PVDF specimen FTIR and WAXD were used. FTIR spectra (Bio-Rad FTIR, FTS 155) were recorded with a resolution of 2 cm^{-1}. The WAXD patterns of PVDF specimens were analyzed using a X-ray diffractometer (D8 X-ray diffractometer, Brucker AXS, Meadowside, UK) with a wavelength of 1.542 Å as X-ray source. The XRD spectra were measured at room temperature from 10 to 50 (2θ) with a step size of 0.028.

Morphology Analyses. SEM images were recorded using a Field Emission Scanning Electron Microscope (Hitachi S-4800) at accelerating voltage of 2.0 kV. AFM (digital Veeco instrument in the tapping mode) was used for investigations of the surface of PVDF films prepared on silica using DMSO as solvent for the polymer.

Results and Discussion

PVDF samples with different end groups were applied to a detailed investigation into polymer properties. End group analyses were carried out by ESI−MS and ^{1}H NMR spectroscopy. The polymers under investigation are listed in Table 1. Number average molecular weights are based on polystyrene calibration of the SEC.

The molecular weight data in Table 1 indicate that $C_6F_{13}I$ is a more efficient CTA than CCl_3Br. While 0.921 mol·L^{-1} CCl_3Br are required to yield polymer with M_n of 2100 g·mol^{-1}, only 0.15 mol·L^{-1} $C_6F_{13}I$ were sufficient to yield similar M_n values.

Positive ESI−MS of PVDF. Electrospray ionization mass spectrometry (ESI−MS) has proven to be a valuable tool for end group analyses of synthetic polymers. Due to the soft ionization fragmentation may be omitted and end group functionalities may fully be retained in the ionized molecules. ESI−MS was applied to a large variety of polymers,[39−42] including some fluoropolymers.[43] Here, ESI−MS was employed to characterize PVDF samples which were subsequently analyzed with respect to morphology and crystallinity. Unlike radical polymerizations of many other monomers chain growth in VDF polymerization predominantly proceeds via head to tail addition.[44] As a consequence termination occurs mainly via combination and contributions from disproportionation may be neglected. Therefore, species originating from bimolecular termination carry two end groups. As long as transfer of hydrogen is unlikely, hydrogen end groups will be scarce.

First, PVDF from reactions with perfluorinated hexyl iodide is considered. Due to the high chain transfer-constant of $C_6F_{13}I$ in VDF polymerizations,[45,46] it was anticipated that chain growth was predominantly stopped by chain transfer events rather than by bimolecular termination with other radicals. In case of transfer being the major chain stopping event only a minor fraction of initiator-derived end groups is expected to be present in the macromolecules. To confirm that transfer is the major chain stopping event ESI−MS spectra were measured. Figure 1 gives such a spectrum for a PVDF sample with $M_n = 2400$ g·mol^{-1} (PFHI-1). The spectrum shows a rather small number of prominent peaks, which are periodically repeated. These peaks are separated by *m*/*z* of 64.03, the molar mass of the VDF monomer. The full spectrum exhibits a shape that is typical for

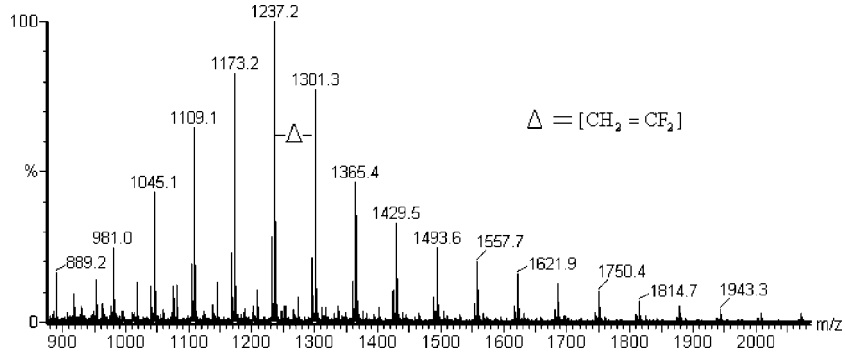

Figure 1. Electrospray mass spectrometry results for poly(vinylidene fluoride) polymerized at 120 °C, 1500 bar initiated by 0.061 mol·L^{-1} di-*tert*-butyl peroxide in the presence of 0.164 mol·L^{-1} $C_6F_{13}I$ (sample PFHI-1 in Table 1).

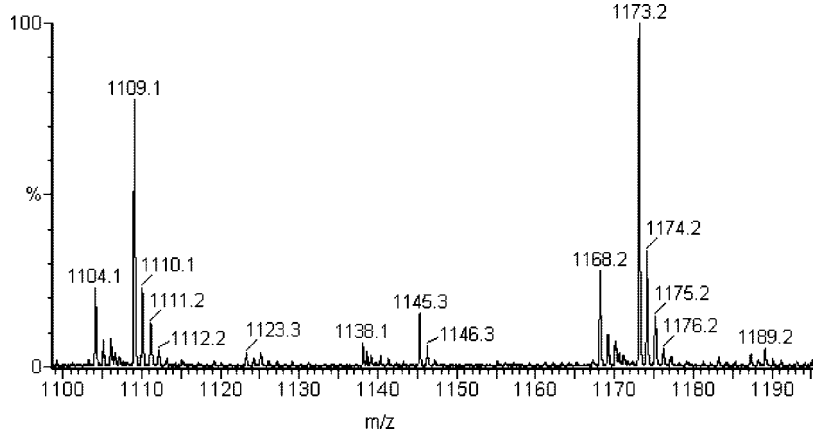

Figure 2. Expansion of the electrospray ionization mass spectrometry results given in Figure 1 for poly(vinylidene fluoride) (PVDF) polymerized at 120 °C, 1500 bar initiated by 0.061 mol·L^{-1} di-*tert*-butyl peroxide (DTBP) in the presence of 0.164 mol·L^{-1} $C_6F_{13}I$ (sample PFHI-1 in Table 1). Prominent peaks at 1109.1 and 1173.2 refer to PVDF with $C_6F_{13}I$-derived end groups. Species carrying DTBP-derived end groups, expected to occur at 1125.3, 1119.3, 1135.5, or 1141.4, are not found.

the mass spectra of polymers produced by radical polymerization. The peak intensities do not quantitatively represent the actual chain-length distribution,[47−49] as the mode of ionization and further experimental parameters may affect mass sensitivity, in particular for low MW material. At higher molecular weights the observed shape is similar to the number distribution of the polymer, which decays toward higher masses. These effects play a minor role upon considering the mass range of one monomer repeat unit, as shown in Figure 2. Ionization generally proceeds via sodium cations. The prominent peak occurring at m/z = 1109.1 is assigned to species consisting of 10 VDF units, which was initiated by C_6F_{13} and terminated by transfer to I. Formally, the mass of 1109.1 could also refer to a species with 7 VDF units that was initiated and terminated by C_6F_{13}, or to a species consisting of 13 VDF units that was initiated and terminated by I. Based on the ESI−MS data a differentiation between these species is not possible. Thus, additional polymerizations were carried out with perfluorinated octyl iodide, $C_8F_{17}I$. Corresponding ESI−MS spectra show prominent peaks at, e.g., m/z = 1439.5 which is unique for species of 13 VDF units carrying a C_8F_{17} and an iodine end group and a sodium cation from ionization. Thus, it may be concluded that using $C_6F_{13}I$ also species are formed, which carry one perfluorinated hexyl group and one iodine atom. This assignment is also in agreement with the finding that the use of $C_6F_{13}I$ leads to living radical polymerization conditions.[27] Considering the livingness of the systems containing $C_6F_{13}I$ M_n values may also be estimated according to $M_n = \alpha_{VDF} \times [C_6F_{13}I]_0/[VDF]_0 \times M_{VDF}$ where α_{VDF} refers to VDF conversion, $[C_6F_{13}I]_0$ and $[VDF]_0$ to the initial concentrations of $C_6F_{13}I$ and VDF, respectively, and M_{VDF} is the molar mass of the monomer.[50] Knowing that complete monomer conversions were reached for PFHI-1 and PFHI-2 M_n values of 2000 and 5300 g·mol^{-1}, respectively, were calculated. These values agree rather well with the SEC-derived values of 2400 and 6700 g·mol^{-1}. The result indicates that SEC data for the low M_n samples are a good estimate of the absolute molecular weights, although polystyrene calibration was used.

PVDF species carrying the DTBP-derived end groups CH_3 or $OC(CH_3)_3$ are expected to occur at m/z = 1125.3 (CH_3 and I or C_6F_{13} as end groups) and at m/z = 1119.3 ($OC(CH_3)_3$ and I or C_6F_{13} as end groups) in Figure 2. The spectrum in Figure 2 indicates that these species are absent. Thus, it may be concluded that chain initiation and chain termination are caused by the chain-transfer agent.

ESI−MS analysis of PDVF samples with DTBP-derived end groups results in more complicated spectra. While still prominent peaks separated by m/z = 64.03 are observed, in between two neighboring peaks a large number of smaller peaks is seen. These peaks may be due to different DTBP-derived end groups. In addition, ESI−MS may also produce multiply charged ions and the ionization process may cause elimination of one or more HF molecules.[43] The latter was not observed for PVDF from reactions in the presence of $C_6F_{13}I$. ESI−MS spectra for PVDF with CCl_3Br-derived end groups were not accessible. Thus, end groups had to be derived from ^{1}H NMR spectra.

End Group Analyses via ^{1}H NMR Spectroscopy. An ^{1}H NMR spectrum of PVDF sample PFHI-1 is given in the upper part of Figure 3 in the spectral window from 0.9 to 4.3 ppm. On the basis of the detailed spectra discussion by the group of Ameduri and Boutevin the ^{1}H NMR spectra may be interpreted as follows:[50] 2.4 ppm is representative of tail to tail addition (−CF_2−C**H**$_2$−CH_2−CF_2−), whereas the peak at 3.0 ppm is assigned to normal head to tail addition (−CH_2−CF_2−C**H**$_2$−

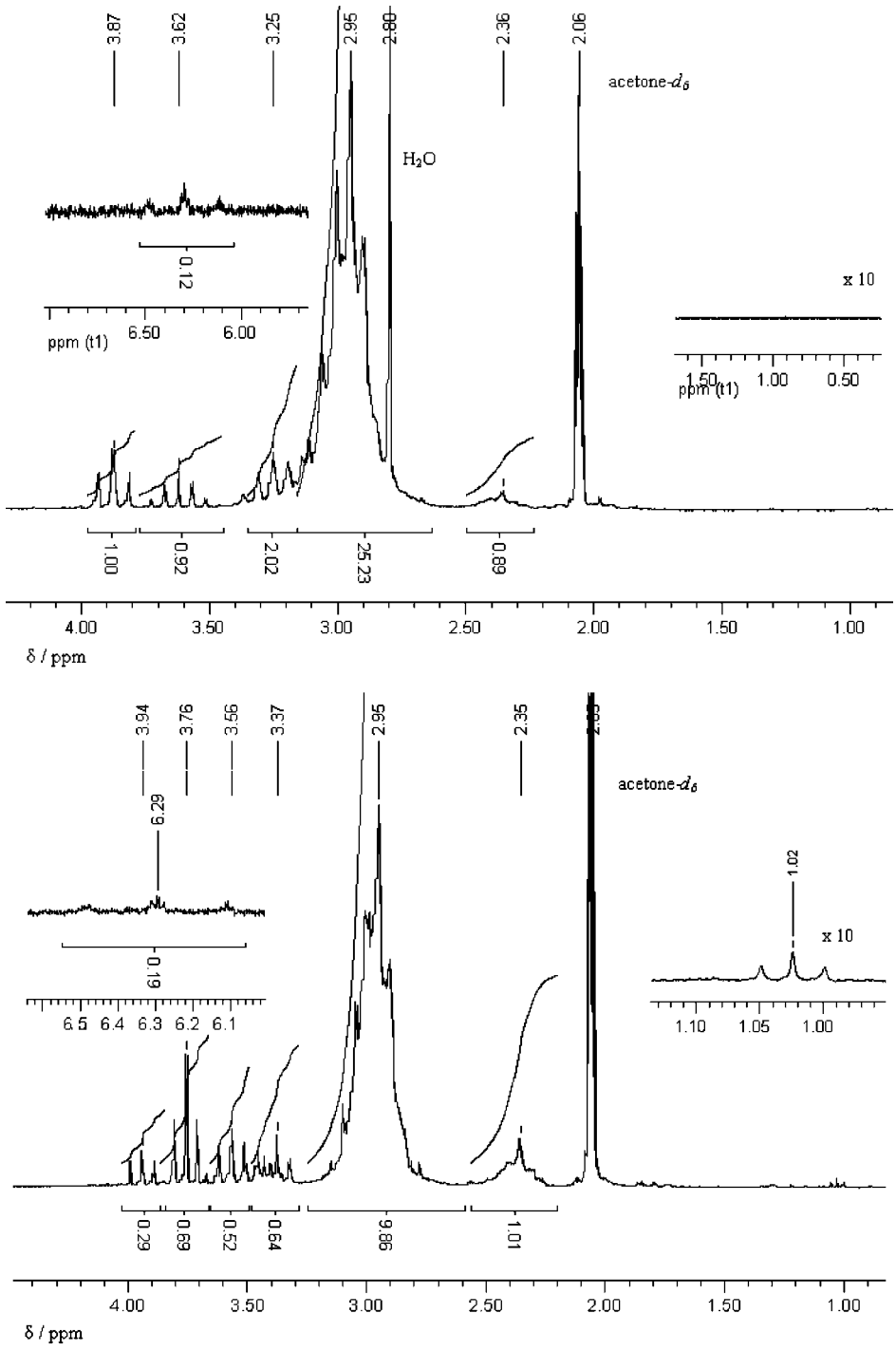

Figure 3. ^{1}H NMR (acetone-d_6) of poly(vinylidene fluoride) polymerized at 120 °C and 1500 bar initiated by 0.077 mol·L^{-1} di-*tert*-butyl peroxide in the presence of 0.164 mol·L^{-1} $C_6F_{13}I$ (upper spectrum, sample PFHI-1 in Table 1) or 0.921 mol·L^{-1} CCl_3Br (lower spectrum, sample BTCM-1 in Table 1) used for analysis of the polymer end groups. The inserts show the area around 1 ppm and around 6.3 ppm after magnification.

CF_2-). The peak at 3.3 ppm may be assigned to $C_6F_{13}-C\mathbf{H}_2-CF_2$ groups. Iodine end groups give rise to peaks at 3.6 and 3.9 ppm, which are assigned to $-C\mathbf{H}_2-CF_2-I$ and $-CF_2-C\mathbf{H}_2-I$, respectively. Acetone as solvent gives rise to a peak at 2.1 and a peak at 2.8 ppm is due to traces of water. Thermal decomposition of DTBP yields *tert*-butoxy radicals, which may initiate polymerization and result in *tert*-butoxy end groups in the polymer. In addition, *tert*-butoxy radicals may undergo elimination of acetone yielding methyl radicals that may initiate polymerization and result in methyl end groups. PVDF species with *tert* butoxy (tBuO) end groups are expected to give rise to a signal at 1.3 ppm referring to the methyl groups in the tBuO-CH_2-CF_2 sequence.[52] Previously, we showed that the formation of tBuO end groups is negligible.[26] Instead two distinct signals centered around 1.0 and 1.8 ppm, which may be assigned to methyl protons in $CH_3-CH_2-CF_2-$ and $CH_3-CF_2-CH_2$, respectively, were observed. This finding of methyl end groups is in accordance with studies into the initiation of VDF polymerizations at 100 °C with DTBP.[52]

The ^{1}H NMR spectrum of sample PFHI-1 in the upper part of Figure 3 indicates that even at a magnification by a factor of 10, as shown in the insert, there are no such contributions from DTBP-derived methyl groups. Thus, the ^{1}H NMR result indicates that DTBP-derived end groups are absent. Consequently, all PVDF chains were initiated and terminated solely by the action of $C_6F_{13}I$.

In addition, PVDF from polymerization with CCl_3Br as chain transfer agent and DTBP as initiator was analyzed by ^1H NMR spectroscopy. The peaks were assigned according to refs 46 and 51. The ^1H NMR spectrum in the lower part of Figure 3 contains the above-mentioned peaks at 2.4 and 3.0 ppm assigned to $-CF_2-C\mathbf{H}_2-CH_2-CF_2-$ and $-CH_2-CF_2-C\mathbf{H}_2-CF_2-$ sequences of the polymer backbone. Additional peaks at 3.8 and 3.6 ppm may be assigned to $CCl_3-C\mathbf{H}_2-CF_2-$ and $-C\mathbf{H}_2-CF_2-Br$ units originating from chain transfer. The weak peaks at 3.4 and 3.9 ppm are representative of $C\mathbf{H}_2-CF_2-Cl$ and $CF_2-C\mathbf{H}_2-Br$, respectively.

For samples PFHI1- and BTCM-1 signals centered at 1.0 ppm characteristic for methyl protons originating from DTBP decomposition are of negligible intensity compared to the other peaks (also illustrated by the 10-fold magnification of the spectrum around 1 ppm given in the insert). Thus, it is concluded that the fraction of initiator-derived end groups is negligible for PVDF from polymerizations with molecular weight control via both chain transfer agents.

In addition to information on the polymer end groups, the ^1H NMR spectra also allow for the detection of significant contributions from chain transfer to polymer resulting in $\mathbf{H}-CF_2-CH_2$ sequences.[52] As discussed in literature these protons give rise to a peak at 6.3 ppm. For PVDF samples with $C_6F_{13}I$- and CCl_3Br-derived end groups the NMR spectra do not show any peak at 6.3 ppm. For PVDF with DTBP-derived end groups a peak of very low intensity is observerd. However, the intensity is too low for obtaining reliable results from spectra integration, since the integral is of similar value as the integral of the baseline calculated for the same range. Thus, it may be concluded that transfer to polymer occurs only to a very low extent, and thus, the high polydispersity of samples DTBP-1 and DTBP-2 is caused by the high DTBP concentrations required for MW control. This explanation is supported by the fact that the polydispersity is significantly larger for the low MW sample. Due to the absence of significant chain transfer to polymer linear chains were obtained.

The results from ESI−MS and ^1H NMR prove that the amount of DTBP-derived end groups is negligible, if polymer molecular weights are controlled by the chain transfer agents CCl_3Br or $C_6F_{13}I$. Of course, polymers obtained from reactions in the absence of any chain transfer agents give rise to DTBP-derived end groups, as previously shown.[26] The predominant end groups of the polymers employed in this study on the morphology of PVDF polymers are listed in Table 1.

Besides allowing for end group analyses, ^1H NMR spectra were used to estimate absolute M_n values and the fraction of the so-called defect structures resulting from tail to tail addition.[52] The M_n values obtained are within 30% of the M_n values derived from SEC employing polystyrene calibration, e.g. the NMR-derived value of M_n for sample PFHI-1 is 2000 $g\cdot mol^{-1}$ compared to 2400 $g\cdot mol^{-1}$ from SEC. The fraction of defect structures amounts to 7% for PFHI-1 and DTBP-1 and to 9.5% for BTCM-1. These numbers are rather high, however, it has to be kept in mind that the polymerizations were carried out up to complete monomer conversion, and consequently more defect structures accumulate than in low conversion polymerizations generally reported in literature. Further, it is noted that the result for BTCM-1 seems to be in conflict with literature results, where no defect structures were reported. However, the published data refer to reactions with a very high concentration of CCl_3Br resulting predominantly in mono- and diadducts. As will be discussed below the extremely high CCl_3Br concentration used in literature also affected the chain transfer constant.[46]

Morphology of PVDF. Visual observation of the PVDF samples listed in Table 1 indicated that different morphologies ranging from fine free-flowing powder to coagulated material were found. To get further information on the morphology SEM images were measured for the samples listed in Table 1. The images obtained for PVDF with M_n between 2100 and 2400 $g\cdot mol^{-1}$ are given in Figure 4. The upper SEM image (a) for sample DTBP-1 shows small stacks of layered material. The size of these stacks is around 10 μm and the particle size distribution is rather narrow. The SEM image in the middle was obtained for PVDF with $C_6F_{13}I$-derived end groups. Here, a sponge-type morphology is observed. Finally, CCl_3Br-derived PVDF end groups result in rather coagulated material that does not show any distinct structures. The observation of these very

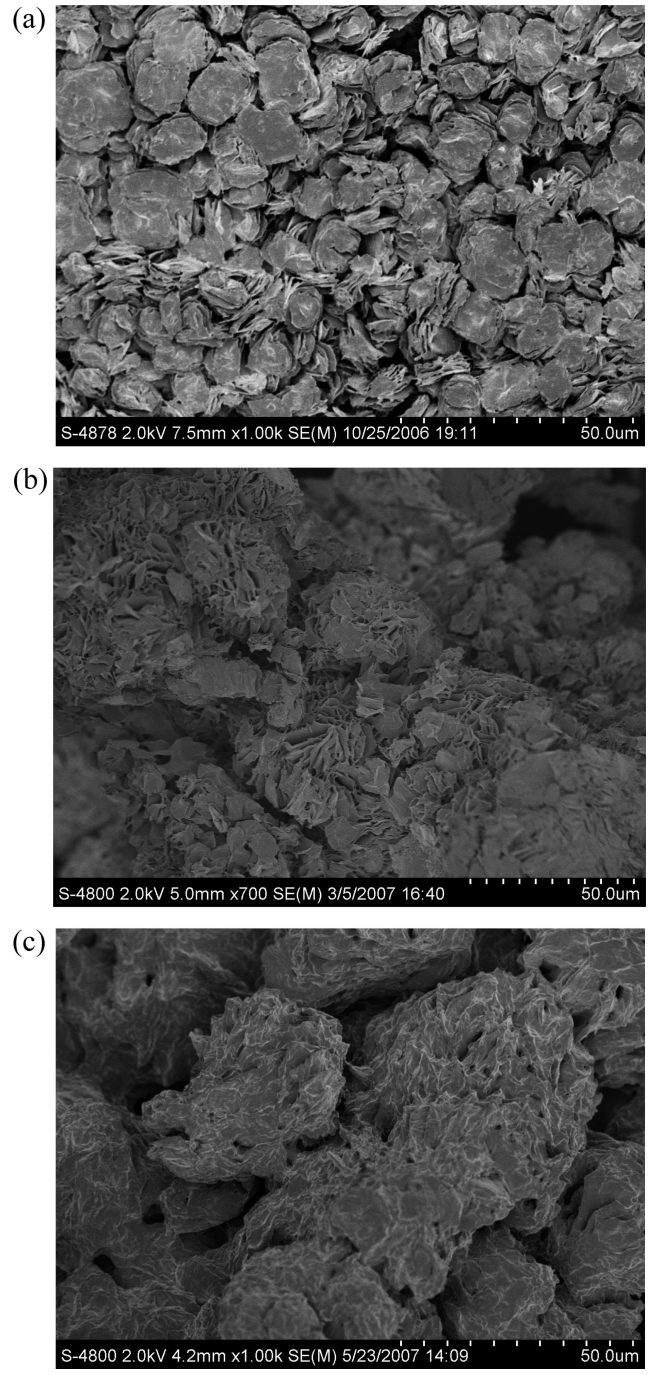

Figure 4. Scanning electron microscopy images of poly(vinylidene fluoride) (PVDF) samples collected after expansion of the reaction mixture at polymerization conditions to ambient conditions. PVDF samples with number average molecular weights range from 2100 to 2400 $g\cdot mol^{-1}$ and end groups originating from di-*tert*-butyl peroxide (a), $C_6F_{13}I$ (b), and CCl_3Br (c).

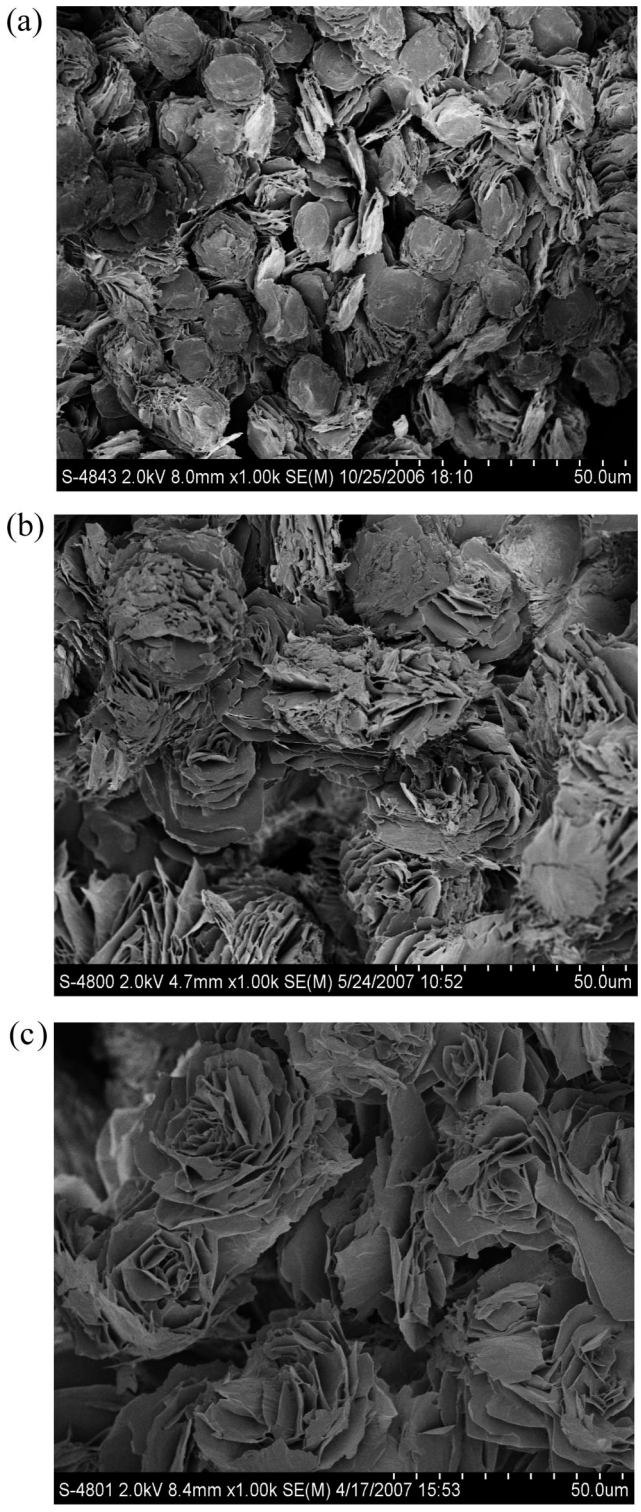

Figure 5. Scanning electron microscopy images of poly(vinylidene fluoride) (PVDF) samples collected after expansion of the reaction mixture at polymerization conditions to ambient conditions. PVDF samples with number average molecular weights between 6000 and 6800 g·mol^{-1} and end groups originating from di-*tert*-butyl peroxide (a), $C_6F_{13}I$ (b), and CCl_3Br (c).

different morphologies is in accordance with the visual impression of the polymers.

It was anticipated that the influence of the polymer end groups is more pronounced for low molecular weight (MW) material than for higher molecular weights. To test whether differences also occur for higher MW material a second set of SEM images shown in Figure 5 was measured for polymers with a M_n ranging

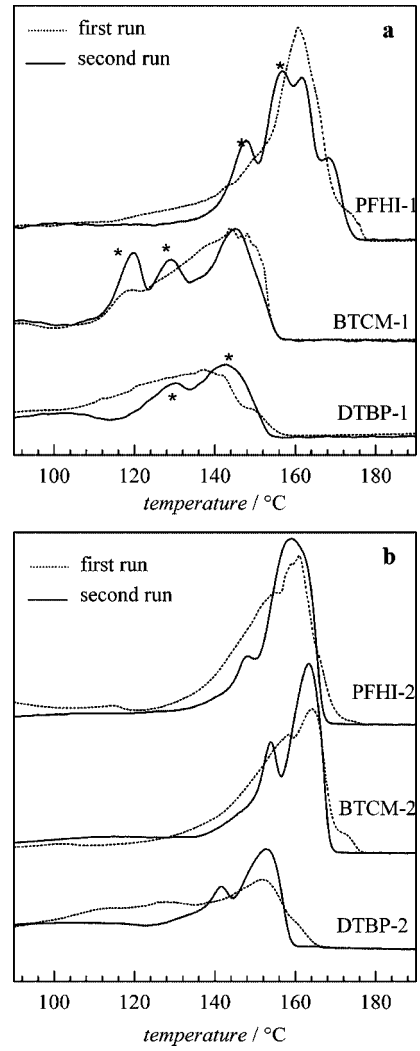

Figure 6. Differential scanning calorimetry results for poly(vinylidene fluoride) samples with different end groups and number average molecular weights, M_n. Dotted lines: first heating cycle, full line: second heating cycle. BTCM-1, BTCM-2: CCl_3Br derived end groups and M_n = 2100 g·mol^{-1}, M_n = 6000 g·mol^{-1}, respectively. DTBP-1, DTBP-2: Di-*tert*-butyl peroxide derived end groups and M_n = 2200 g·mol^{-1}, M_n = 6800 g·mol^{-1}, respectively. PFHI-1, PFHI-2: $C_6F_{13}I$ derived end groups and M_n = 2400 g·mol^{-1}, M_n = 6700 g·mol^{-1}, respectively.

from 6000 to 6800 g·mol^{-1}. As expected the images of the three polymers seem to be less different. In all cases material with small-scale morphology is found. Again, for DTBP-derived end groups stack-type particles are observed, which are not significantly different from the particles for the low MW sample of Figure 4. Using $C_6F_{13}I$ as transfer agent also results in polymer with lamellar structures. In case of CCl_3Br as transfer agent small rose patel like structures, having a diameter of around 25 μm, are seen. In contrast, the low MW polymer (BTCM-1) resulted in rather undifined material.

DSC and Crystallinity. The SEM images indicate that polymer end groups as well as polymer molecular weights influence polymer morphology upon expansion to ambient conditions. To understand why the above-described differences in morphology occur, the degree of crystallinity of the polymer samples was investigated applying DSC. Figures 6a and 6b give the heating curves of the low and high MW samples, respectively.

From literature it is well-known that the morphology of PVDF may be varied by many experimental parameters, e.g., such as the speed of cooling,[53] the CO_2 pressure or the pressure at which

Table 2. Results from Differential Scanning Calorimetry[a]

sample	T_m^I (°C)	T_m^{II} (°C)	T_c (°C)	ΔH_m (J·g^{-1})	X (%)
PFHI-1	149.4[b]	156.7[b]	123.6	65.3	62
BTCM-1	120.3[b]	130.6[b]	104.9	44.2	42
DTBP-1	130.7	142.7	117.8	27.2	26
PFHI-2	148.1	158.9	131.2	67.2	64
BTCM-2	154.1	163.5	130.0	50.7	49
DTBP-2	141.6	152.6	109.5	30.0	29

[a] Melting temperatures, T_m^I, T_m^{II} refer to the first and second peak maximum observed in the second heating cycle. [b] T_m^I and T_m^{II} as indicated by the stars in Figure 6a. T_c: crystallization temperature, ΔH_m: melting enthalpy; X: crystallinity calculated according to eq. 1.

crystallization occurs.[2,54,55] In addition, the polymers obtained upon expansion from CO_2/polymer mixtures to ambient pressure may contain varying amounts of CO_2 dissolved in the polymer. Moreover, in contrast to most PVDF crystallization studies generally reported in literature, expansion of CO_2/polymer mixtures is a process, in which large temperature and pressure changes occur very rapidly, typical values are 10^7 bar·s^{-1} and 10^9 K·s^{-1}.[56] As a consequence expansion may give rise to heterogeneous material. Thus, it seemed important to measure two heating cycles. Due to crystallization of the material in the DSC instrument at a constant cooling rate of 10 °C/min the samples employed in the second heating run underwent identical treatment prior to melting. In parts a and b of Figure 6, the curves from the first heating cycle are represented by the dotted line and the second cycle by the full line. Generally, the first heating curve is less structured than the second. First, the DSC results of the low MW samples depicted in Figure 6a are considered. The curves from the second heating cycle are almost as broad as the first curves. For sample BTCM-1, which showed the undefined structure in the SEM image, the temperature range for melting extends from around 110 to 155 °C. Material with DTBP-derived end groups melts at slightly higher temperature. For $C_6F_{13}I$-derived end groups the temperature range for melting is the highest and starts at around 140 °C. The DSC results for the higher MW samples are depicted in Figure 6b. As for the low MW material the first heating cycles result in less structured curves, which show indications of bimodality. For all three samples the second heating cycle results in well resolved bimodal curves. The temperature range for melting is very similar for BTCM-2 and PFHI-2. Sample DTBP-2 melts at slightly smaller temperatures. For comparison the two peak maxima are listed in Table 2. For the low MW samples the peaks marked with a star in Figure 6a are listed.

For comparison with literature the melting temperatures of the higher MW samples are considered. The first melting temperature, T_m^I, lies between 141.6 and 154.1 °C, the second melting temperature, T_m^{II}, between 152.6 and 163.5 °C. Typical melting temperatures for high MW α phase PVDF are in the range of 163 °C. Recently, also bimodal DSC curves were reported for PVDF. A peak around 165 °C was assigned to β phase material and a peak around 173 °C to α phase material.[38] In contrast, Gegorio reported that the melting temperature of α and β phase material determined by DSC is not significantly different.[57] The occurrence of different DSC peaks for α phase PVDF was assigned to the mode of crystallization, rapid crystallization by temperature quenching or slow crystallization at isothermal conditions. Moreover, Shieh et al. reported that the size of the crystallites influences the DSC heating curve, and that multimodal crystal size distributions result in broad DSC curves.[2] Already this small selection of potential influences on the DSC curves indicates that an assignment of the peaks observed to the various polymorphs of PVDF seems not advisable.

However, the DSC results allow for the calculation of the degree of crystallinity, X. To allow for the calculation of X according to $X = \Delta H_m/\Delta H_c$ the melting enthalpy, ΔH_m, was determined by integration of the DSC curve of the second heating cycle. The results are listed in Table 2. $\Delta H_c = 104.5$ J·g^{-1} for perfectly crystalline PVDF was used to calculate X, assuming that the heat of fusion for both crystalline forms is the same for 100% crystalline material.[38] For the low MW samples, the highest melting enthalpy of 65 J·g^{-1} associated with a crystallinity degree of 62% is found for PFHI-1, whereas for DTBP-derived end groups (DTBP-1) a melting enthalpy of 27 J·g^{-1} and a crystallinity of 26% was derived. It is interesting to note that the most massive and heavy chain end groups give rise to the highest melting temperature, which suggests that the entropy of melting decreases with an increase in the weight of the chain end group, because of suppression of the chain mobility by the heavy chain end group in the melt. Table 2 indicates that the melting temperature is higher for the higher MW samples. In contrast to the observation for the crystallinity, this enhancement is not uniform. For comparison T_m^{II} is considered: For $C_6F_{13}I$-derived end groups corresponding to samples with highest crystallinity at each MW, the increase in T_m^{II} is only 2.2 °C. For CCl_3Br-derived end groups T_m^{II} increases by 32.9 °C and for DTBP-derived end groups by 9.9 °C. The findings for T_m are paralleled by the crystallization temperatures, T_c, derived from the cooling curves. All cooling curves show a single sharp peak. Different cooling scans of a single sample do not result in significant differences. The T_c values are contained in Table 2. Keeping the end group constant and increasing M_n yields an increase in T_c for low polydispersity samples with $C_6F_{13}I$- and CCl_3Br-derived end groups: For CCl_3Br-derived end groups T_c increases by 25 °C, whereas for $C_6F_{13}I$-derived end groups T_c is enhanced by 8 °C upon increasing M_n. In contrast the samples with DTBP-derived end groups show a lowering in T_c by 8 °C upon increasing molecular weight. However, it has to be noted that the low MW sample shows a significantly higher polydispersity, which is expected to lead to a lowering in the crystallization temperature for the lower MW sample.

Since the first and second heating curves show close proximity it may be concluded that the differences in crystallinity observed for the samples with different end groups are not due to the expansion process but are inherent to the constitution of the PVDF material. While the degree of crystallinity may be derived from DSC analysis, the unambiguous assignment of the types of polymorphs present is not possible. To determine the different PVDF crystal phases FTIR and WAXD analyses were applied.

Polymorphs of PVDF. The different crystalline phases of PVDF are distinguished by the conformation of the C−C bonds along the polymer main chain. The α phase has alternating trans and gauche bonds (TGTG), the β phase has all trans bonds (TTTT), the γ phase has a gauche bond every fourth repeat unit (T_3GT_3G), and the δ phase is very similar to the α-crystalline phase except that every other chain is rotated.[58] As reported in literature, the different crystalline phases may be distinguished by differences in their IR spectra.[57,59−62] The characteristic bands of the α phase are 530 cm^{-1} (CF_2 bending), 615 and 765 cm^{-1} (CF_2 bending and skeletal bending), 796 cm^{-1} (CH_2 rocking), 976 cm^{-1} (CH_2 twisting) and a peak at 1178 cm^{-1}. The β phase is associated with absorptions at 510 cm^{-1} (CF_2 bending) and 840 cm^{-1} (CH_2 rocking). Absorptions at 512, 776, 812, 833 and 840 cm^{-1} are characteristic for the γ phase.

Figure 7 gives IR spectra of samples PFHI-1, BTCM-1 and DTBP-1. The absorptions at 763 and 795 cm^{-1} characteristic for α phase PVDF are clearly seen in all samples. The IR spectrum of sample BTCM-1 shows two peaks at 717 and 938 cm^{-1} not seen in the other spectra. The peaks may be assigned to CCl_3 and Br as polymer end groups, respectively.[63] The

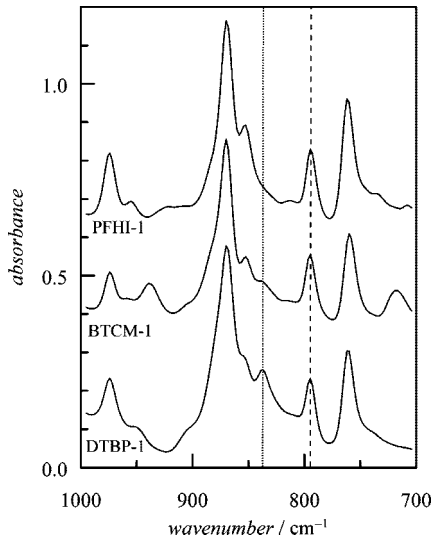

Figure 7. Fourier transform infrared spectra of poly(vinylidene fluoride) samples with number average molecular weights between 2100 and 2400 g·mol^{-1} and end groups originating from the initiator di-*tert*-butyl peroxide (DTBP-1), from $C_6F_{13}I$ (PFHI-1), and from CCl_3Br (BTCM-1).

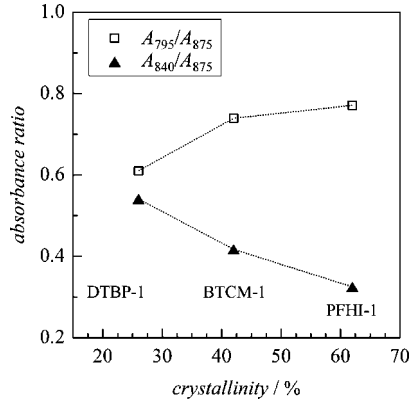

Figure 8. Absorbance ratios A_{795}/A_{875} and A_{840}/A_{875} as calculated from Fourier Transform Infrared spectra given in Figure 7. A_{795}, A_{840} and A_{875} are the absorbances at 795 cm^{-1}, 840 cm^{-1}, and 875 cm^{-1}, respectively.

characteristic band at 840 cm^{-1} (indicated by the dotted line), that may be assigned to the β and γ phase, is present in all spectra, whereas the bands at 776, 812 and 833 cm^{-1} characteristic for the γ phase are absent in all three samples. Thus, it may be anticipated that the peak at 840 cm^{-1} refers to the β phase. As previously reported the band at 875 cm^{-1} (CH_2 bending) is observed for α and β phase polymorphs and may be used as an internal standard for comparison of different spectra.[2] The ratios of A_{795}/A_{875} and A_{840}/A_{875} provide information on the fraction of α and β polymorphs contained in the sample. A_{795}, A_{840} and A_{875} are the absorbances at 795 cm^{-1}, 840 cm^{-1}, and 875 cm^{-1}, respectively. Figure 8 gives the ratios of A_{795}/A_{875} and A_{840}/A_{875} derived from the IR spectra as a function of the degree of crystallinity (lines serve as visual guides). The diagram indicates that the lowest degree of crystallinity is associated with the least differences in the ratio of A_{795}/A_{875} and A_{840}/A_{875}: The differences in the fraction of α and β phase material present in the sample are the lowest. The ratio A_{795}/A_{875} and thus the amount of α crystal phase present in the sample are enhanced as the overall crystallinity increases. These changes are associated with a decrease in the β phase ratio as overall crystallinity is increasing. It should be noted,

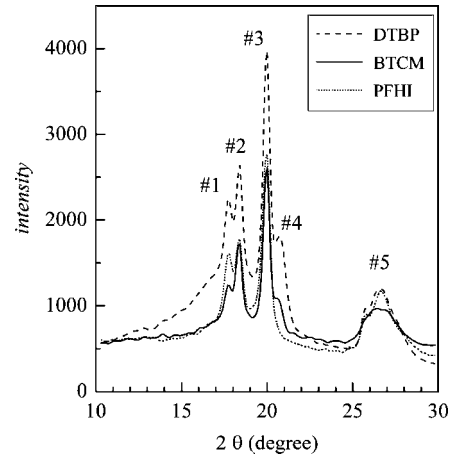

Figure 9. Wide angle X-ray diffraction spectra of poly(vinylidene fluoride) samples with number average molecular weights between 2100 and 2400 g·mol^{-1} and end groups originating from the initiator di-*tert*-butyl peroxide (DTBP-1), from $C_6F_{13}I$ (PFHI-1), and from CCl_3Br (BTCM-1). The acronyms refer to Table 1, where further details are given.

that the ratios do not refer to percentages of α or β phase material.

FTIR spectra recorded for the high MW samples are very similar to the corresponding low MW spectra in Figure 7. Generally, the absorption at 840 cm^{-1} is slightly weaker than for the low MW samples indicating that the fraction of α phase material is enhanced with increasing molecular weight.

Analysis of the absorptions at 840 cm^{-1} and 795 cm^{-1} in Figure 8 indicated that the lowest fraction of β phase material was found for the rather large iodine end group. Literature information on the influence of polymer end groups on the polymorphs of PVDF is scarce. One article reports that iodine end groups give rise to α phase material, contributions from β phase material were not considered.[37] Qualitatively, this result is in agreement with our finding that the lowest fraction of β crystal phase occurs for PVDF with an iodine end group. To confirm the assignments of our IR absorption peaks to α and β phase PVDF, additional wide-angle X-ray diffraction analyses were carried out.

Wide Angle X-ray Diffraction: (WAXD). According to Lovinger[64] the diffraction peaks of (1 0 0), (0 2 0), and (1 1 0) of the α form appear at 17.4, 18.6, 19.5, while the diffraction peak of the β form appears at 20.5 and the diffraction peak of the γ form appears at 14.8. The spectra shown in Figure 9 clearly indicate no significant contributions from the γ phase, which confirms the above-given peak assignment of the FTIR absorptions. Further, the diffraction peaks shown in Figure 9 indicate a predominant occurrence of the α phase, since contributions from the β phase are weak as shown by the rather small diffraction peak at 20.4 − 21.1 (#4). The ratio of the intensities of peaks #1, #2 and #3 assigned to the α phase are very similar for PVDF with DTBP or PFHI-derived end groups, whereas peaks #2 and #3 are more intense for sample BTCM-1. The biggest difference, however, is seen for #4 assigned to the β phase. According to Lovinger, the diffraction peaks of (1 0 0) and (2 0 0) corresponding to the β-phase polymorph overlap at 20.7. The sharpness of this diffraction peak (#4) is found to decrease with increasing β-phase, indicating that the degree of crystallinity of PVDF decreases. While a strong diffraction peak at 20.68 is seen for PVDF with DTBP- and BTCM-derived end groups, this peak is rather weak for PFHI-1. To analyze the WAXD spectra the intensity of the diffraction peak at 26.2 − 26.7 (#5)° for the α phase and at 20.4 − 21.1 (#4)° for the β phase are considered. To characterize the α phase peak #5 was

used rather than peaks #1, #2 or #3, since #5 is more isolated showing a flat baseline which increases the accuracy of the intensity determination. While very similar intensities for the α phase are found for DTBP and BTCM-derived end groups, PFHI-1 shows a slightly higher intensity. Conversely, PFHI shows the weakest intensity of peak #4 in comparison to the other two samples. This finding is in excellent agreement with the results from FTIR, which also indicated lower amounts of β phase in both PFHI samples.

AFM Images of PVDF. Since morphologies after expansion of the reaction mixture as well as crystallinity and the content of α and β phase were strongly affected by the type of end group, it seemed rewarding to examine the surface morphology and the 3D topology applying AFM. Sample preparation for AFM required the dissolution of the polymer in DMSO and subsequent evaporation of the solvent. As detailed above, DSC analyses showed that differences in crystallinity of the samples remain even after several melt and crystallization cycles. Thus, sample preparation for AFM measurements is not expected to eliminate differences due to the polymer end groups.

The AFM images of the low MW samples are given in Figure 10. In all cases no homogeneous coverage of the substrate was achieved. The images indicate some organization of the polymer leading to different patterns on the surface. As can be seen in Figure 10a, the surface of the PFHI-1 sample is rather smooth with distinct indentations leading to round flower-like structures with overall diameters of roughly 20 μm. The average height of the structure is in the order of 4 nm. In case of DTBP-derived end groups the AFM image in Figure 10 b shows two mostly flat circles, which have a diameter of around 4 μm and an average height of 4 nm, as observed for the material with $C_6F_{13}I$-derived end groups. In contrast to the image in Figure 10 a, in the center of these cyclic structures some spikes are seen. Even more spikes are visible in the AFM image for the BTCM-1 sample depicted in Figure 10 c, which make it difficult to identify the surface structure. However, again spherical structures are seen and the height of the material is below 10 nm. It may be concluded that the surface is not as flat and smooth as for the other two samples. This finding is in agreement with the SEM image of sample BTCM-1, which showed no clear structure.

Despite the differences observed in Figure 10a−c, in all cases round structures with diameters being below 25 μm and a thickness below 10 nm were obtained. The formation of flat-on lamella as shown in parts a and b of Figure 10 was reported for crystallization from films with a thickness below 300 nm. For films thinner than 15 nm it was observed that they tend to break-up and form dendritic structures.[65] The AFM images shown in Figure 10 indicate that not only the film thickness, but also the polymer end groups significantly affect the surface morphology of PVDF deposited on a substrate. The formation of structures as shown in Figure 10a for PVDF with $C_6F_{13}I$-derived end groups were assigned to dewetting phenomena.[66] The break-up of the PVDF films is in accordance with the generally weak cohesion energies of fluoropolymers.

The spikes seen on the surfaces may be artifacts, since AFM measurements were carried out using routine procedures. However, since spikes are almost absent for sample PFHI-1, the polymer with the lowest fraction of β phase material, and since it was shown that AFM may be used to study the ferrolectricity of PVDF[67] or to polarize ferroelectric domains,[68] it cannot be excluded that the spikes are due to interactions between the piezoelectric material and the cantilever.

The results reported indicate that polymer end groups have a significant influence on polymer morphology, the ratio of α and β phase material, the overall degree of crystallinity, melting and crystallization temperature as well as the film formation on silica. For example, based upon choice of end groups and molecular weight, PVDF with overall degrees of crystallinity

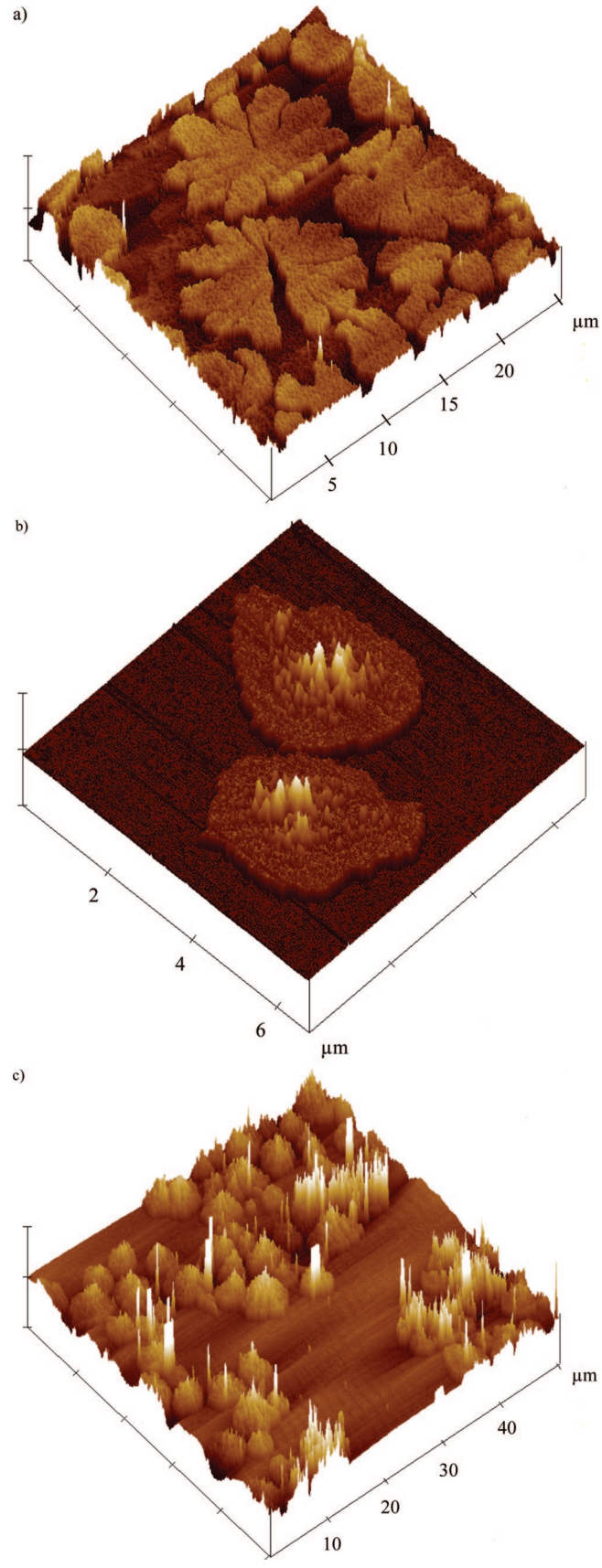

Figure 10. Atomic force microscopy images of the surface of poly(vinylidene fluoride) samples with number average molecular weights around 2200 g·mol^{-1} and end groups originating from $C_6F_{13}I$ (a), di-*tert*-butyl peroxide (b) and CCl_3Br (c).

ranging from 26 to 64% are accessible. The differences in melting and crystallization temperatures remained even after three heating cycles. Although rather low molecular weight material was used, the lower MW samples still consisted of polymer molecules containing around 30 monomer units (estimated from M_n) and the higher MW samples of polymer molecules with 91 to 104 monomer units. In addition, it should be noted that the end group induced differences are larger than the changes induced by molecular weight. To obtain more insight into the factors affecting the PVDF properties, future experiments will be carried out with, e.g., polymers of higher MW and with additional end groups.

Conclusions

The properties of PVDF may largely be affected by the type of polymer end groups. It was shown that polymer morphology, the ratio of α and β phase material, the overall degree of crystallinity, melting and crystallization temperature as well as the film formation on silica may be affected. For example, the choice of end group and molecular weight gives access to PVDF with degrees of crystallinity ranging from 26 to 64%. The highest fraction of β crystal phase material was observed for end groups originating from the initiator di-*tert*-butyl peroxide, whereas $C_6F_{13}I$-derived end groups lead to the lowest fraction of β phase material. Further, AFM results show that thin films in the range of nanometers were obtained on silica. The type of end groups determines the structure of these films.

Acknowledgment. The authors gratefully acknowledge Dyneon, Germany. Dr. Ines Starke (University of Potsdam) is gratefully acknowledged for the ESI−MS analysis. We are grateful to Prof. Dr. Markus Antonietti and his co-workers from MPIKG Golm for WAXD, DSC and FTIR analyses.

References and Notes

(1) Lu, F. J.; Hsu, S. L. *Macromolecules* **1986**, *19*, 326.
(2) Shieh, Y-T.; Hsiao, T.-T.; Chang, S-K. *Polymer* **2006**, *47*, 5929.
(3) Lovinger, A. J. *Macromolecules* **1981**, *14*, 322.
(4) Kosmynin, B. P.; Gal'Perin, E. L. *Vvsokomol. Soedin., Ser. A* **1972**, *A14*, 1603.
(5) Matsushige, K.; Takemura, T. *J. Polym. Sci., Polym. Phys. Ed.* **1978**, *16*, 921.
(6) Gupta, D. K.; Doughty, K. *J. Appl. Phys.* **1978**, *49*, 4601.
(7) Davis, G. T.; McKinney, J. E.; Broadhurst, M. G.; Roth, S. C. *J. Appl. Phys.* **1978**, *49*, 4998.
(8) Kochervinskii, V. V. *Crystallogr. Rep.* **2003**, *48*, 649.
(9) Dang, T.-M.; Wang, L.; Yin, Y.; Zhang, Q.; Lei, Q.-Q. *Adv. Mater.* **2007**, *19*, 852.
(10) Chen, Y.; Deng, Q.; Xiao, J.; Nie, H.; Wu, L.; Zhou, W.; Huang, B. *Polymer* **2007**, *48*, 7604.
(11) Mokrini, A.; Huneault, M. A.; Gerard, P. *J. Membr. Sci.* **2006**, *283*, 74.
(12) Reverchon, E.; Cardea, S. *Ind. Eng. Chem. Res.* **2006**, *45*, 8939.
(13) Giesy, J. P.; Kannan, K. *Environ. Sci. Technol.* **2001**, *35*, 1339.
(14) Wood, C. D.; Yarbrough, J. C.; Roberts, G.; DeSimone, J. M. In *Supercritical Carbon Dioxide in Polymer Reaction Engineering*; Kemmere, M. F., Meyer, T., Eds.; Wiley-VCH: Weinheim, Germany, 2005; pp 189−204.
(15) Beginn, U.; Najjar, R.; Ellmann, J.; Vinokur, R.; Martin, R.; Moeller, M. *J. Poly. Sci., Part A: Polym. Chem.* **2006**, *44*, 1299.
(16) Mueller, P. A.; Storti, G.; Morbidelli, M.; Costa, I.; Galia, A.; Scialdone, O.; Filardo, G. *Macromolecules* **2006**, *39*, 6483.
(17) Ahmed, T. S.; DeSimone, J. M.; Roberts, G. W. *Macromolecules* **2008**, *41*, 3086.
(18) Ahmed, T. S.; DeSimone, J. M.; Roberts, G. W. *Macromolecules* **2007**, *40*, 9322.
(19) Ahmed, T. S.; DeSimone, J. M.; Roberts, G. W. *Macromolecules* **2006**, *39*, 15.
(20) Kennedy, K. A.; Roberts, G. W.; DeSimone, J. M. *Adv. Polym. Sci.* **2005**, *175*, 329.
(21) Saraf, M. K.; Gerard, S.; Wojcinski, L. M.; Charpentier, P. A.; DeSimone, J. M.; Roberts, G. W. *Macromolecules* **2002**, *35*, 7976.
(22) Liu, J.; Tai, H.; Howdle, S. M. *Polymer* **2005**, *46*, 1467.
(23) Tai, H.; Wang, W.; Howdle, S. M. *Macromolecules* **2005**, *38*, 9135.
(24) Tai, H.; Wang, W.; Howdle, S. M. *Polymer* **2005**, *46*, 10626.
(25) Tai, H.; Wang, W.; Martin, R.; Liu, J.; Lester, E.; Licence, P.; Woods, H. M.; Howdle, S. M. *Macromolecules* **2005**, *38*, 355.
(26) Beuermann, S.; Imran-ul-haq, M. *J. Polym. Sci., Part A. Polym Chem.* **2007**, *45*, 5626.
(27) Beuermann, S.; Imran-ul-haq, M. *Macromol. Symp.* **2007**, *259*, 210.
(28) Kirby, C. F.; McHugh, M. A. *Chem. Rev.* **1999**, *99*, 565.
(29) Kazarian, S. G.; Vincent, M. F.; Bright, F. V.; Liotta, C. L.; Eckert, C. A. *J. Am. Chem. Soc.* **1996**, *118*, 1729.
(30) Mawson, S.; Johnston, K. P.; Combes, J. R.; DeSimone, J. M. *Macromolecules* **1995**, *28*, 3182.
(31) Su, B.; Lu, X.; Yang, Y.; Ren, Q. *J. Chem. Eng. Data* **2006**, *51*, 542.
(32) Kilic, S.; Michalik, S.; Wang, Y.; Johnson, J. K.; Enick, R. M.; Beckman, E. J. *Macromolecules* **2007**, *40*, 1332.
(33) Lora, M.; Lim, J. S.; McHugh, M. A. *J. Phys. Chem. B* **1999**, *103*, 2818.
(34) Dinoia, T. P.; Conway, S. E.; Lim, J. S.; McHugh, M. A. *J. Polym. Sci., Part B. Polym. Phys.* **2000**, *38*, 2832.
(35) Briscoe, B. J.; Lorge, O.; Wajs, A.; Dang, P. *J. Polym. Sci., Part B. Polym. Phys.* **1998**, *36*, 2435.
(36) Scheirs, J., Ed. *Modern Fluoropolymers, High Performance Polymers for Diverse Applications*; Wiley: New York, 1997.
(37) Herman; Uno, T.; Kubono, A.; Umemoto, S.; Kikutani, T.; Okui, N. *Polymer* **1997**, *38*, 1677.
(38) Neidhöfer, M.; Beaume, F.; Ibos, L.; Bernes, A.; Lacabanne, C. *Polymer* **2004**, *45*, 1679.
(39) Hanton, S. D. *Chem. Rev.* **2001**, *101*, 527.
(40) Buback, M.; Frauendorf, H.; Günzler, F.; Vana, P. *J. Polym. Sci., Part A: Polym. Chem.* **2007**, *45*, 2453.
(41) Szablan, Z.; Lovestead, T. M.; Davis, T. P.; Stenzel, M. H.; Barner-Kowollik, C. *Macromolecules* **2007**, *40*, 26.
(42) Quan, C. L.; Soroush, M.; Grady, M. C.; Hansen, J. E.; Simonsick, W. J. *Macromolecules* **2005**, *38*, 7619.
(43) Marie, A.; Fournier, F.; Tabet, J. C.; Ameduri, B.; Walker, J. *Anal. Chem.* **2002**, *74*, 3213.
(44) Duc, M.; Ameduri, B.; Boutevin, B.; Kharroubi, M.; Sage, J. M. *Macromol. Chem. Phys.* **1998**, *199*, 1271.
(45) Boyer, C.; Valade, D.; Lacroix-Desmazes, P.; Ameduri, B.; Boutevin, B. *J. Polym. Sci., Polym. Chem. Ed.* **2006**, *44*, 5763.
(46) Duc, M.; Ameduri, B.; David, G.; Boutevin, B. *J. Fluorine Chem.* **2007**, *128*, 144.
(47) Axelsson, J.; Scrivener, E.; Haddleton, D. M.; Derrick, P. J. *Macromolecules* **1996**, *29*, 8875.
(48) Hunt, S. M.; Sheil, M. M.; Belov, M.; Derrick, P. J. *Anal. Chem.* **1998**, *70*, 1812.
(49) Zammit, M. D.; Davis, T. P.; Haddleton, D. M.; Suddaby, H. G. *Macromolecules* **1997**, *30*, 1915.
(50) Boyer, C.; Valade, D.; Sauget, I.; Ameduri, B.; Boutevin, B. *Macromolecules* **2005**, *38*, 10353.
(51) Pianca, M.; Barchiesi, E.; Eposto, G.; Radice, S. *J. Fluorine Chem.* **1999**, *95*, 71.
(52) Guiot, J.; Ameduri, B.; Boutevin, B. *Macromolecules* **2002**, *35*, 8694.
(53) Yang, D.; Chen, Y. *J. Mater. Sci. Lett.* **1987**, *6*, 599.
(54) Koga, Y.; Saito, H. *Polymer* **2006**, *47*, 7564.
(55) Hattori, T.; Kanaoka, M.; Oigashi, H. *J. Appl. Phys.* **1996**, *79*, 2016.
(56) Türk, M. *J. Supercrit. Fluids* **2000**, *18*, 169.
(57) Gregorio, R.; Cestari, M. *J. Polym. Sci., Part B: Polym. Phys* **1994**, *32*, 859.
(58) Hsu, S. L.; Lu, F. J.; Waldman, D. A.; Muthukumar, M. *Macromolecules* **1985**, *18*, 2583.
(59) Tashiro, K.; Kobayashi, M.; Tadokoro, H. *Macromolecules* **1981**, *14*, 1757.
(60) Benedetti, E.; Catanorchi, S.; D'Alessio, A.; Moggi, G.; Vergamini, P.; Pracella, M.; Ciardelli, F. *Polym. Int.* **1996**, *41*, 35.
(61) Benz, M.; Euler, W. B. *J. Appl. Polym. Sci.* **2003**, *89*, 1093.
(62) Peng, Y.; Wu, P. *Polymer* **2004**, *45*, 5295.
(63) Hesse, M.; Meier, H.; Zeeh, B. *Spektroskopische Methoden in der organischen Chemie*; Thieme: Stuttgart, Germany, 1987.
(64) Lovinger, A. J. *Polymer* **1980**, *21*, 1317.
(65) Chan, C.-M.; Li, L. *Adv. Polym. Sci.* **2005**, *188*, 1.
(66) Reiter, G. *J. Polym. Sci., Part B: Polym. Phys.* **2003**, *41*, 18697.
(67) Noda, K.; Ishida, K.; Kubono, A.; Horiuchi, T.; Yamada, H.; Matsushige, K. *Jpn. J. Appl. Phys* **2001**, *40*, 4361.
(68) Kimura, K.; Kobayashi, K.; Yamada, H.; Horiuchi, T.; Ishida, K.; Matsushige, K. *Appl. Phys. Lett.* **2003**, *82*, 4050.

MA801325P